Available online at www.sciencedirect.com
SCIENCE DIRECT
Polymer 46 (2005) 439–444
polymer
www.elsevier.com/locate/polymer

Microscopic mechanism of reinforcement in single-wall carbon nanotube/polypropylene nanocomposite

T.E. Chang[a], L.R. Jensen[b], A. Kisliuk[a], R.B. Pipes[c], R. Pyrz[b], A.P. Sokolov[a,*]

[a]*Department of Polymer Science, University of Akron, Akron, OH 44325, USA*
[b]*Institute of Mechanical Engineering, Aalborg University, Aalborg East DK9220, Denmark*
[c]*Department of Polymer Engineering, University of Akron, Akron, OH 44325, USA*

Received 1 September 2004; received in revised form 9 November 2004; accepted 17 November 2004

Abstract

We analyzed mechanical properties and structure of polypropylene fibers with different concentrations of single-wall carbon nanotubes (SWNTs) and draw down ratios (DDR). Tensile tests show a three times increase in the Young's modulus with addition of only 1 wt% SWNT, and much diminished increase of modulus with further increase in SWNT concentration. Microscopic study of the mechanism of reinforcement by SWNT included Raman spectroscopy and wide-angle X-ray diffraction (WAXD). The results show linear transfer of the applied stress from the polymer matrix to SWNT. Analysis of WAXD data demonstrates formation of a β-crystal phase in polypropylene matrix under the strain.

Keywords: Carbon nanotubes; Polypropylene; Microscopic mechanism

[1]. Introduction

Experimental and theoretical investigations suggest [1–8] that carbon nanotubes (CNT) have remarkable mechanical properties with Young's modulus values and elastic bending modulus of single-wall nanotubes ropes being in the order of TPa [9,10,12] and tensile strength as high as 200 GPa [11]. These extraordinary mechanical properties and high aspect ratio make carbon nanotubes ideal reinforcing agent in nanocomposite materials. The potential of carbon nanotubes for application as structure reinforcement, however, depends on the ability to disperse the nanotubes homogeneously throughout the matrix and on a transfer of the mechanical load from the matrix to the nanotubes. Significant enhancement of mechanical properties of epoxy resins [6,13–17], thermoplastics polymer [18,19], poly(methyl methacrylate) (PMMA) [20], polyethylene (PE) and polystyrene (PS) [21] has been achieved with addition of CNT. However, the microscopic mechanism of polymer reinforcement by carbon nanotubes has not been understood yet.

One of the methods to analyze microscopic load transfer from the matrix to the nanotubes is the use of the Raman spectroscopy [6]. It has been demonstrated that the position of the second-order Raman band at 2610 cm^{-1}, the so-called D*-band, shifts with applied strain or stress [22,23]. If the stress applied to composite material is transferred to CNT, the Raman peak shifts by a few cm^{-1}. This shift varies linear with applied strain, and the slope of the frequency–strain response depends on the orientation of the nanotubes and on the properties of polymer matrix [24,25].

In this work, influence of single-wall carbon nanotubes (SWNT) on the mechanical properties of the polypropylene (PP) fibers is studied. Microscopic structure of composites is analyzed using Raman scattering and wide angle X-ray diffraction (WAXD). Strong reinforcement (threefold increase) is achieved at rather low concentrations of SWNT. Stress versus strain curves show non-linear behavior that is ascribed to changes in crystallinity of the PP fibers under the stretching. SWNT's Raman peak exhibits non-linear shift with strain, but exhibits linear

* Corresponding author. Tel.: +1 330 972 8409; fax: +1 330 972 5290.
E-mail address: alexei@uakron.edu (A.P. Sokolov).

0032-3861/$ - see front matter © 2004 Elsevier Ltd. All rights reserved.
doi:10.1016/j.polymer.2004.11.030

variations with stress. The results suggest that the PP-matrix transfers stress effectively to SWNT.

[2]. Experimental

[2.1]. Fabrication of SWNT-PP fibers

The SWNT materials from Carbolex Inc. were sonicated in 80 ml decahydronaphthalene with a Misonix Inc. high-power sonicator for ~30 min. The sonication was accomplished in a pulse mode in order to avoid excessive heating of the solution and evaporation of the solvent. After 30 min sonication, the carbon nanotube—decahydronaphthalene solution was placed on a hot plate and heated to 140 °C.

Polypropylene granules (from Basell Polyolefins with a HG455FB grade) were added to the solution at $T=140$ °C and dissolved by mechanical stirring at this temperature for 45 min. The solution became highly viscous when the PP was added and further use of the sonicator was not possible. The so-obtained gel-like solution was poured onto aluminum foil and placed in a vacuum oven at 150 °C at an absolute pressure of 0.34 bar for ~7 h in order to dry the material. After drying, the material was left to cool to ambient and then was broken into small pieces of ~5–8 mm that could be used as pellets in the fiber spinning process.

The fibers were spun using an Instron capillary rheometer with a die diameter of 1.6 mm followed by a collection of the fiber on a high speed take up device. The piston speed of the capillary rheometer was varied between 0.76 and 25.4 mm/min while the speed of the take up devices was varied up to 125 rpm. By varying the speeds of the rheometer and take up device the draw down ratio (DDR) of the fiber could be controlled. The draw down ratio of the different fibers was measured using an optical stereomicroscope. The composite fibers were prepared with several SWNT concentrations specified as weight percentages in the polymer: 1, 2, 3, 4, and 5 wt%. Small traces of decahydronaphthalene have been found in the dried fibers by TGA.

[2.2]. Measurements

Measurements of stress–strain curves of the composite fibers have been performed using a mini-tensile testing machine. Strain was varied on time scale of seconds, however, the strain rate cannot be controlled. The mini-tensile testing machine was placed in the Raman spectrometer or X-ray device, so stress–strain behavior and Raman or WAXD data were measured at the same time. Raman and WAXD measurements usually took a few minutes and stress relaxation smaller than 10% was observed during the measurements. Therefore, tensile strength was calculated from the averaged value of the measured force divided by the cross-section area of the fiber samples.

Raman scattering spectra of the SWNT-PP fibers were measured in backscattering geometry with Jobin Yvon T64000 triple monochromator. A Krypton laser with a wavelength of 647 nm and power of 4 mW was used as an excitation source. The samples were placed in the mini tensile device for measurement at various levels of strain. For estimation of the SWNT orientation, the tangential mode of the SWNT in Raman spectrum was measured at 0 and 90° between the fiber axis and the polarization of light direction. The Raman spectrum for each direction has been measured in three different points of the same sample in order to average out possible inhomogeneity in dispersion of SWNT in the fiber.

The WAXD measurements were carried out with a Rigaku 12 kW rotating anode X-ray (Cu Kα radiation) generator equipped with a diffractometer at 50 kV and 200 mA. Samples were scanned in a 2θ-angle range between 1.5 and 35° using 2D detector. An air scattering pattern with no sample was also collected and used for background correction of the WAXD data. All measurements were performed at room temperature.

[3]. Results

Fig. 1 shows the stress–strain behavior of pure PP fiber and PP composite fibers containing different SWNT concentrations. Young's moduli defined as the stress–strain ratio in the low strain region are presented in Fig. 2 as a function of the SWNT concentration. The tensile modulus of the fibers increases sharply (~3 times) with addition of 1 wt% SWNTs. However, it increases much slower with further addition of SWNT (Fig. 2). Tensile stiffness increased only ~45% when concentration of SWNT increases from 1 to 4–5 wt%. Another observation is a change of the slope of the stress–strain curve for strains above ~0.8–1.0% (Fig. 1) that was observed in all samples including pure PP. The stress–strain measurements of fibers

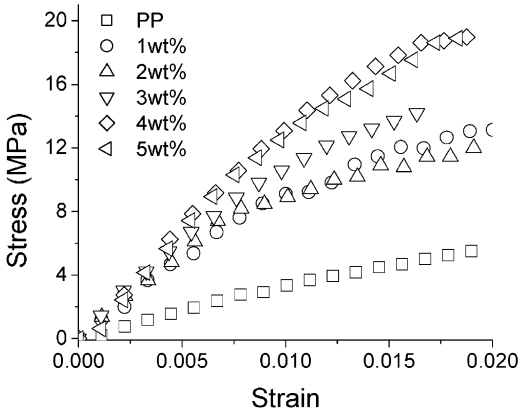

[Fig. 1]. Stress–strain curves of pure PP and PP composite fibers with different concentrations (DDR = 110).

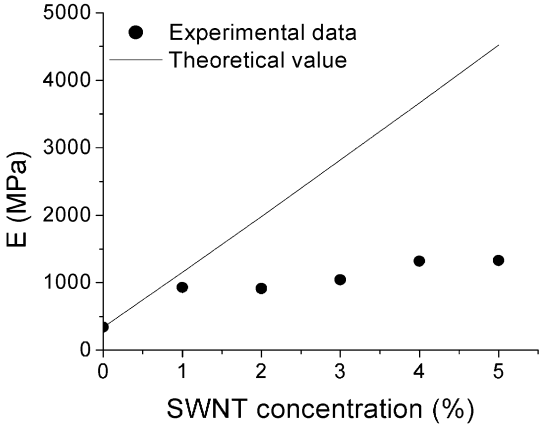

[Fig. 2]. Dependence of the Young's modulus on concentration of SWNT: symbols—experimental results, the solid line is theoretical calculation using the eq. 1.

obtained with different draw down ratio (DDR) showed no dependence of Young's modulus on DDR.

Fig. 3(a) shows the circularly integrated 1D WAXD intensity profiles of the pure PP fiber at various strains (0, 0.5, 1.0 and 2.0%). The neat PP initial pattern without strain (0%) shows the typical α-form PP crystals and no changes are observed at 0.5% strain. However, when the PP fiber is stretched further (1 and 2%), the peak near 16° becomes double peak suggesting appearance of β-form of PP [26]. The same behavior is obtained in the SWNT/PP composite fiber, which is shown in Fig. 3(b).

It is known that tangential Raman mode at $\nu \sim 1500$–$1600\ \mathrm{cm}^{-1}$ is sensitive to the orientation of carbon nanotubes relative to polarization of light [21,27]. Fig. 4 shows the Raman spectra of the 2 wt% SWNT/PP composite fiber with DDR of 87. All spectra were normalized to the intensity of the PP peak at $\nu \sim 1450\ \mathrm{cm}^{-1}$ (which does not show dependence on fiber orientation relative to polarization of light). The Raman scattering intensity of the

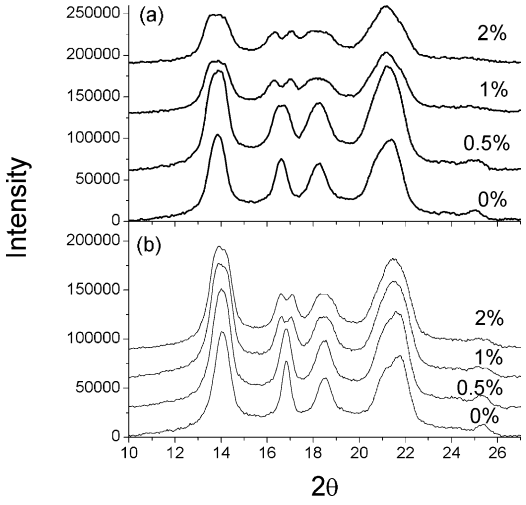

[Fig. 3]. Changes of wide angle X-ray diffraction under strain (shown by numbers) in (a) pure PP and (b) PP-1% SWNT.

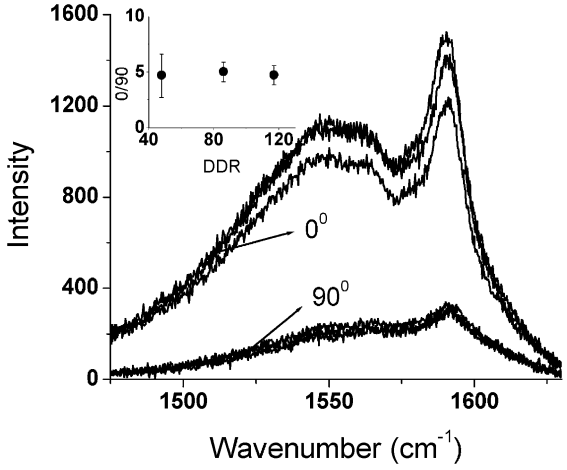

[Fig. 4]. Raman spectra of tangential mode measured at different points in PP—2 wt% SWNT composite fiber (DDR = 87). The angle between fiber axis and polarization of incident light are 0 degree (top 3 spectra) and 90 degree (bottom 3 spectra). Inset shows dependence of the ratio of the integrated intensities of the mode measured at two orientations on DDR.

SWNT mode decreases significantly when the angle between the fiber axis and polarization of light changes from 0 to 90°, suggesting preferential orientation of SWNT along the fiber direction. Degree of orientation was calculated as a ratio of integrated Raman intensities measured at 0 and 90°. The orientation factor was seen to be ~5 with no significant dependence on DDR or concentration of SWNT (inset Fig. 4).

Raman spectroscopy has also been used to analyze the load transfer from the matrix to the nanotubes [6]. Frequency of SWNT D*-band is sensitive to stress and is often used as a stress sensor [22]. Fig. 5 shows the spectra of D*-band of the sample containing 1 wt% SWNT with no strain and with 2% strain. The mode shifts to lower frequency under tensile stress. The D*-band peak was fit by a Lorentzian curve to estimate the position of its maximum. The peak position of the D*-band is seen to shift to a lower value on application of a tensile strain. The initial slopes are approximately $-200\ \mathrm{cm}^{-1}$ per strain with no significant

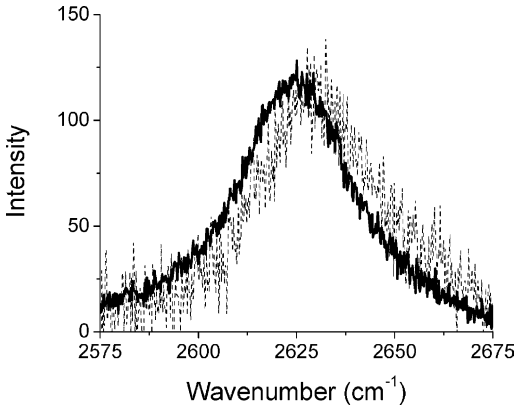

[Fig. 5]. The Raman spectra of D*-mode in PP—1 wt% SWNT composite with no strain (dashed line) and with 2% strain (solid line).

dependence on concentration or DDR (Fig. 6). These data demonstrate clear transfer of the load to SWNTs. The data also show change in the slope at strain above ~0.8–1.0%.

To check reversibility of the properties under extension, one of the fibers with 2 wt% SWNT and 117 DDR has been loaded to strain ~2%, then unloaded and left to relax over night and then loaded again. Results for the stress–strain behavior (Fig. 7(a)) and the shift of the Raman peak (Fig. 7(b)) show complete reversibility.

[4]. Discussion

The presented results show transfer of the mechanical load from PP-matrix to SWNT that appears to be rather independent of concentration and DDR. Also orientation of SWNT and the Young's modulus appear to be independent of DDR. Recent studies of PE-SWNT fibers found dependence of CNT orientation and modulus on DDR [21]. One of the reasons for this difference might be rather narrow DDR range studied in our work: we vary DDR less than three times while more than 30-fold variations were studied in [20,21].

The Young's modulus shows an interesting dependence on SWNT concentration (Fig. 2): strong increase with addition of 1 wt% and rather weak increase with further addition of SWNT up to 5 wt%. A decrease of reinforcing rate with filler concentration above a certain amount has been observed for many composite materials [28–31]. If the SWNT-PP composite fibers are assumed as randomly oriented discontinuous fiber lamina, the composite modulus E_c, can be calculated according to the following equation [32].

$$E_c = \left[\frac{3}{8}\frac{1+2(l_{NT}/d_{NT})\eta_L V_{NT}}{1-\eta_L V_{NT}} + \frac{5}{8}\frac{1+2\eta_T V_{NT}}{1-\eta_T V_{NT}}\right]E_{pp}$$

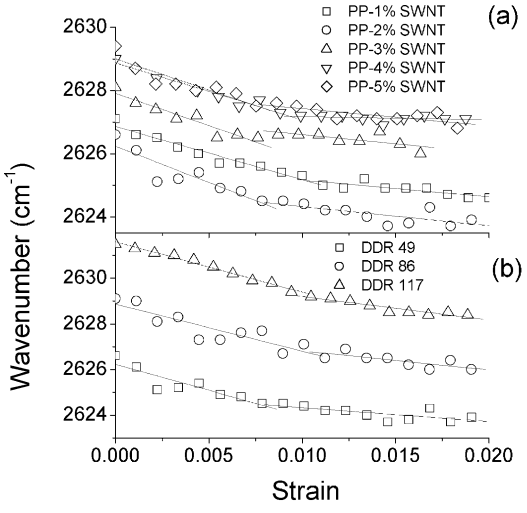

[Fig. 6]. Dependence of the D*-band peak position on strain (a) for fibers with different concentrations of carbon nanotubes and the same DDR ~ 110; (b) for PP—2 wt% SWNT with different DDR.

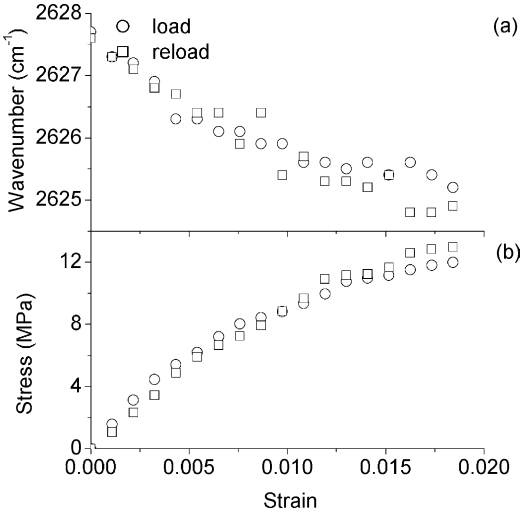

[Fig. 7]. Results of loading and reloading the sample of PP—2 wt% SWNT with DDR = 117: (a) stress–strain curve and (b) dependence of the D*-band peak position on strain.

$$\eta_L = \frac{(E_{NT}/E_{PP})-1}{(E_{NT}/E_{PP})+2(l_{NT}/d_{NT})}, \quad \eta_T = \frac{(E_{NT}/E_{PP})-1}{(E_{NT}/E_{PP})+2}$$

where E_{pp} and E_{nt} represent tensile modulus of pure PP and SWNT, V_{nt} the volume fraction of SWNTs, l_{nt}/d_{nt} is their aspect ratio. We calculate the expected modulus taking density of PP and SWNT equal to 0.9 and 1.34 g/cm^3 [33], respectively, and assuming aspect ratio ~1000 and modulus E_{nt} ~ 600 GPa [33] for SWNT. The theoretical calculation and experimental values for the Young's modulus are compared in Fig. 2. Experimental value at 1 wt% is in good agreement with the theoretical calculation (Fig. 2). However, at increasing nanotube concentrations, the deviation is greater. This behavior might be explained as the poor distribution of SWNT that becomes even more heterogeneous with increase in concentration.

The stress–strain curves for composites with various SWNT concentration and DDR exhibit change of the slope at strain ~0.8–1.0% (Fig. 1). The nanotube slippage in the polymer matrix under stress has been reported in recent papers [34,35]. This could explain the observed change of slope in stress–strain curves (Fig. 1). However, similar behavior is also observed in the pure PP fibers. WAXD data (Fig. 3) provide another explanation—change of PP crystallinity under stress. It is known that isotactic polypropylene have four different crystalline structures, corresponding to monoclinic (α), hexagonal (β), triclinic (γ), and smectic or quenched polymorphs. The monoclinic structure is usually obtained under typical industrial and laboratory processing conditions, while the β-form can be obtained under particular thermal condition and under shear stress [26,36]. The mechanical properties such as Young's modulus and yield stress of PP reduce slowly with an increase in the β-phase content [37]. WAXD data show (Fig. 3) that the β-crystal of the PP is formed when fibers are uniaxially stretched. Therefore, stretching of the composite

above some level (strain higher than ~0.8–1.0%) leads to formation of the β-crystals in PP matrix, which causes decrease in modulus and change in the stress–strain behavior.

This conclusion is supported by analysis of the Raman spectra (Fig. 6). They also show changes of slope of the shift versus strain at the same value of strain ~0.8–1.0%. However, shift varies linear with the applied stress (Fig. 8). So, there is no slippage of SWNT in PP matrix, but the modulus of the matrix changes under extension due to formation of β-crystals. It has been found that addition of CNT to polypropylene does not change crystallinity of the polymer, although affects crystallization rate [38–41]. Formation of β-crystals apparently happens at the same strain in neat PP and in PP-SWNT composite (Fig. 3) suggesting no significant influence of SWNT on strain-induced transformation of crystalline PP. This result might be not surprising assuming that SWNT are excluded from PP-crystals.

Our results show initial shift of D*-band $-205\pm 30\ \mathrm{cm}^{-1}$/strain. Wagner and co-workers reported shift of the SWNT D*-band $-467\ \mathrm{cm}^{-1}$/strain in UV cured urethane acrylate polymer and various values (between -1422 and $-1800\ \mathrm{cm}^{-1}$/strain) in epoxy resins [25,42,43]. It appears that the shift per strain increases with increase of the matrix modulus ($E\sim 0.35$ GPa in PP, $E\sim 1.2$ GPa in urethane and $E\sim 1.6$–3 GPa in epoxy) suggesting that it depends mostly on the stress transferred from the matrix to SWNT.

Our results also show (Fig. 6) dependence of the initial position of the D*-band on concentration of SWNT and DDR. In all cases, the initial position appears at frequency higher than the position of D*-band in SWNT powder, $\nu\sim 2610\ \mathrm{cm}^{-1}$ [22]. When nanotubes are embedded in a polymer, thermal strain builds up as a consequence of the thermal expansion mismatch between the two phases. Thermal strain that put nanotubes under compression increases the frequency of the D* peak.

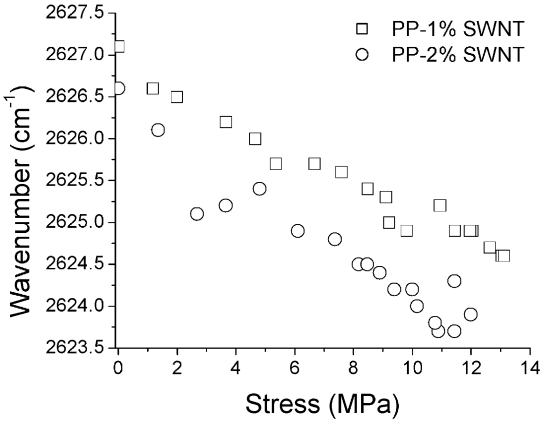

[Fig. 8]. Dependence of the D*-band peak position on stress in PP composite fibers with 1 and 2 wt% SWNT.

[5]. Conclusions

We achieve ~3 times increase in Young's modulus of PP fibers adding only 1 wt% of SWNT. The theoretical calculation of this composite (1 wt%) shows an agreement with experimental value. However, increase in the modulus becomes weaker with further increase of SWNT concentration. Analysis of Raman scattering spectra shows load transfer from polymer matrix to SWNT. The observed stress–strain and Raman band shift–strain curves show the change of the slope when applied strain becomes larger than ~0.8–1%. These changes are ascribed to formation of β-crystal under strain as evidenced by WAXD measurements. The change of crystallinity in the composite fibers under the stress affects the mechanical properties. Shift of the Raman mode varies linear with stress supporting the earlier suggestions that SWNT can be used as stress sensors.

Acknowledgements

This work has been supported in part by grants from Air Force (#F49620-02-1-0428). We thank A.J. Jing for help with X-ray measurements.

References

[1] Despres JF, Deguerre E, Lafdi K. Carbon 1995;33:87.
[2] Treacy MMJ, Ebbesen TW, Gibson JM. Nature (London) 1996;381:678.
[3] Overney G, Zhong W, Tomanek Z. Phys D 1993;27:93.
[4] Robertson DH, Brener DW, Mintmire JW. Phys Rev B 1992;45:12592.
[5] Chopra NG, Benedict LX, Crespi VH, Cohen ML, Louie SG, Zettl A. Nature (London) 1995;377:135.
[6] Wagner HD, Lourie O, Feldman Y, Tenne R. Appl Phys Lett 1998;72:188.
[7] Iijima S, Brabec C, Maiti A, Bernholc J. J Chem Phys 1996;104:2089.
[8] Lourie O, Wagner HD. J Mater Res 1998;13:2418.
[9] Wong EW, Sheehan PE, Lieber CM. Science 1997;277:1971.
[10] Poncharal P, Wang ZL, Ugarte D, de Heer WA. Science 1999;283:1513.
[11] Meyyappan M, Han J. Prototype Tech Int 1998;6:14.
[12] Salvetat JP, Andrew G, Briggs D, Bonard JM, Basca RR, Kulik AJ. Phys Rev Lett 1999;82:944.
[13] Sandler J, Shaffer MSP, Prasse T, Bauhofer W, Schulte K, Windle AH. Polymer 1999;40:5967.
[14] Ajayan PM, Stephan O, Colliex C, Trauth D. Science 1994;265:1212.
[15] Schadler LS, Giannaris SC, Ajayan PM. Appl Phys Lett 1998;733842.
[16] Lourie O, Wagner HD. Appl Phys Lett 1998;73:3527.
[17] Lourie O, Cox DM, Wagner HD. Phys Rev Lett 1998;81:1638.
[18] Jin L, Bower C, Zhou O. Appl Phys Lett 1998;73:1197.
[19] Bower C, Rosen R, Jin L, Han J, Zhou O. Appl Phys Lett 1999;74:3317.
[20] Haggenmueller R, Gommans HH, Rinzler AG, Fischer JE, Winey KI. Chem Phys Lett 2000;330:219.
[21] Haggenmueller R, Zhou W, Fischer JE, Winey KI. J Nanosci Nanotechnol 2003;3:105.
[22] Wood JR, Zao Q, Frogley MD, Meurs ER, Prins AD, Peijs T, Dunstan DJ, Wagner HD. Phys Rev B 2000;62:7571.

[23] Wood JR, Wagner HD. Appl Phys Lett 2000;76:2883.
[24] Wood JR, Frogley MD, Meurs ER, Prins AD, Peijs T, Dunstan DJ, Wagner HD. J Phys Chem B 1999;10:10388.
[25] Wood JR, Zao Q, Wagner HD. Compos, Pt A 2001;32:391.
[26] Ellis G, Gomez MA, Marco C. The internet journal of vibrational spectroscopy, vol. 5, 4th ed. Section 5.
[27] Saito R, Takeya T, Kimura T, Dresselhaus G, Dresselhaus MS. Phys Rev B 1998;57:4145.
[28] Gordeyes SA, Ferreira JA, Bernardo CA, Ward IM. Mater Lett 2001; 51:32.
[29] Carneiro OS, Maia JM. Polym Compos 2000;21(6):970.
[30] Carneiro OS, Maia JM. Polym Compos 2000;21(6):960.
[31] Feller JF, Linossier I, Grohens Y. Mater Lett 2002;57:64.
[32] Mallick PK. Fiber-reinforced composites. New York: Marcel Dekker; 1993.
[33] http://www.wag.caltech.edu/foresight/foresight_2.html.
[34] Schadler LS, Giannaris SC, Ajayan PM. Appl Phys Lett 1998;73: 3842.
[35] Ajayan PM, Schadler LS, Giannaris C, Rubio A. Adv Mater 2000;12: 750.
[36] Varga J, Karger-Kocsis J. Polym Bull 1993;30:105.
[37] Tordjeman Ph, Robert C, Marin G, Gerard P. Eur Phys J E 2001;4: 459.
[38] Bhattacharyya AR, Sreekumar TV, Liu T, Kumar S, Ericson LM, Hauge RH, Smalley RE. Polymer 2003;44:2373.
[39] Valentini L, Biagiotti J, Kenny JM, Santucci S. J Appl Polym Sci 2003;87:708.
[40] Grady BP, Pompeo F, Shambaugh RL, Resasco D. J Phys Chem B 2002;106:5852.
[41] Sandler J, Broza G, Nolte M, Schulte K, Lam YM, Shaffer MSP. J Macromol Sci B 2003;B42:479.
[42] Zhao Q, Frogley MD, Wagner HD. Compos Sci Technol 2001;61: 2139.
[43] Zhao Q, Frogley MD, Wagner HD. Polym Adv Technol 2002;13:759.